)

Optical characterization of different module technologies

Rita Ebner, Bernhard Kubicek, Gusztav Újvári and Karl Berger

Photovoltaic Systems (PVS), Energy Department, AIT Austrian Institute of Technology, Giefinggasse 2, 1210 Vienna, Austria

E-mail: rita.ebner@ait.ac.at

For a complete quality control of different module technologies (crystalline and thin film) a combination of fast and non-destructive methods was investigated. Camera-based measurements, such as electroluminescence (EL), photoluminescence (PL), and infrared (IR) technologies, offer excellent possibilities for determining production failures or defects in solar modules, which cannot be detected by means of standard power measurements. These types of optical measurement provide high resolution images with a two-dimensional distribution of the characteristic features of PV modules. This paper focuses on quality control and characterization using EL, PL, and IR imaging with conventional cameras and an alternative excitation source for the PL-setup.

)

1. Introduction

Electroluminescence (EL), photoluminescence (PL) and infrared (IR) imaging are non-destructive measurement techniques. These types of optical measurement provide fast, real-time and high resolution images with a two-dimensional distribution of the characteristic features of photovoltaic (PV) modules. These technologies are applied effectively in quality control and development support and are important characterization tools in industry and research. In previous works, a combination of EL and IR measurements were proposed in order to quickly detect the most common defects in a PV module with high accuracy[1-4]. In this work a combination of EL, PL, and IR characterization tools are presented with the aim to increase the number of detectable defects and to determine their origin.

2. Theory

2.1 IR thermography

By means of IR measurements the thermal behavior of cells in a module and a number of defects (e.g., short-circuits in solar cells, shunts, inactive cell parts, moisture, and defective bypass diodes) can be determined[5,6].

IR measurements can be taken by using an external current or by applying light[7-9]. During measurements in the dark, no light is applied to the module but an external current [less than or equal to the short-circuit current (I_{sc})] is supplied in forward direction. In a previous work it was shown that dark thermography compared to illuminated thermography is a better tool for thin-film modules. Dark thermography images of thin film modules offer more detail and a better defect resolution compared to illuminated thermography images.

In order to avoid thermal damaging in thin film modules, it has to be observed that the short circuit current of the module is not exceeded. For low voltages, below the threshold voltage of the diode, the current flows through the parallel resistance (R_p) and the series resistance (R_s). As $R_s < R_p$, the heating is mainly due to shunted areas. For voltages over the threshold, a large amount of the current flows through the diode itself and heats up the diode and the series resistance[4].

By means of an appropriate IR camera, the temperature distribution can be identified and

compared to EL and PL measurements. Thermography imaging at Austrian Institute of Technology (AIT) was performed by means of a portable, uncooled IR camera. The wavelength of the used IR detector is between 7.5 and 15 µm. As the front plate of all measured PV modules consists of a glass plate with a thickness of 3-4 mm, and thus is only transparent for detectors with a wavelength of 3 to 5 µm, only the temperature of the glass surface can be measured and not the radiation coming directly from the solar cells.

2.2 Dark lock-in thermography

Dark lock-in thermography (DLIT) is a further non-destructive test method[10]. For DLIT, pulsed current is applied to the solar cell without illumination. Then, only the dark current flows within the cell. At shunt sites, an increased current causes heating of the solar cell which can be easily detected by LIT. The variations in temperature are in the area of one-tenth degree. The Fourier analysis of the local variations in temperature can be characterized as sinus wave with amplitude and phase. The ground frequency amplitude image gives information about the intensity of the heating sources in a module.

The DLIT was mainly developed for the detection of shunts[11]. Noises, resolution and contrast of DLIT analysis depend on the used excitation frequency as well as on the recording time. By means of a cooled microbolometer based IR-camera and a power supply unit, a DLIT system was built up. DLIT can be used for detailed failure analysis.

2.3 EL measurements

EL measurements take advantage of the radiative inter-band recombination of excited charge carriers in solar cells. For EL investigations, a solar cell is operated as a light emitting diode. Due to recombination effects, the emitted radiation can be detected with a sensitive CCD camera. The wavelength window of the used Si-CCD-camera is 300 to 1000 nm.

The solar cells are supplied with a defined external excitation current [current applied $\leq$ short circuit current (I_{sc}) of the cell or module] while the camera takes an image of the emitted photons. Damaged areas of a solar module appear dark or radiate less than areas without defects and lighter EL intensity means more electroluminescent output. EL has proven to be a useful tool for investigating electrical inhomogeneities caused by intrinsic defects (e.g., grain boundaries, dislocations, shunts or other process failures) and extrinsic

)

defects (e.g., cell cracks, TCO corrosion or interrupted contacts)[12-16]. The high resolution of the EL-images enables to resolve some defects more precisely than in IR-images[17,18].

To determine the influence of defects (e.g., shunts) the EL behavior of modules when applying different current densities was investigated. With a low current density (~1/10 of the I_{sc} of the cell or module) the conductivity of shunts is very high. The stronger the shunts are, the lower is the EL intensity in this area. Strong shunts are able to quench the EL intensity of a whole cell. When applying higher current densities (~I_{sc} of the cell or module), the conductivity of the pn-junction increases compared to the shunt conductivity, and shunts are less influential on the EL intensity distribution[19,20]. Thus, with low current densities, the material properties, and, with high current densities, the properties of the electrical contacts can be investigated.

2.4 PL-imaging

PL imaging is, compared to EL imaging, a contactless and non-destructive measurement technique[21-23]. As no electric contacts are required, PL can be applied to solar cells before and after each processing stage[24].

The combination of PL imaging with EL imaging of finished cells gives further information about cell performance losses (e.g., resistance losses).

In PL imaging systems commonly high power lasers are used to generate excess charge carriers, and an InGaAs CCD camera works as detector. But as this equipment has a limited resolution an alternative equipment was searched for[25]. Light emitting diode (LED) arrays turned out to be a very cost efficient alternative excitation source, and further, a cooled Si-CCD camera was used instead of an InGaAs camera. The PL system built up at AIT consists of a sensitive Si-CCD camera (300 to 1000 nm wavelength window) and innovative IR LED arrays with a peak wavelength of □□= 850 nm (see Fig. 1). The LED spectrum was chosen to have a negligible overlap with the luminescence spectrum (950-1200 nm). In our setup the camera is placed on the same side as the LED arrays. This requires a good filtering as a large portion of the excitation light is reflected on the wafer and strikes the camera. This is performed by a two-step filter, of which one is a custom-made anti-reflex-coated GaAs wafer, which is transparent in the range of the emitted PL photons. The second filter is a normal LP950 optical filter in front of the

camera. The PL-setup as well as the EL setup at AIT are consisting of an automatic control system, featuring a custom made auto-focus system. The problem is that the focus for visible and IR is different, and PL exposure times can be larger than 30 s. As manual focusing would be resource consuming, a computer-controlled system was created for this task. The measure for the sharpness is the average deviation of pixel brightness, and the approach occurs by a trisection algorithm, similar to normal binary dissection methods.
The PL setup as well as the EL setup at AIT consist of an automatic control system, featuring a custom made autofocus system.

3. Experiments

Crystalline solar cells and crystalline an thin film solar modules were analyzed by electroluminescence, photoluminescence (in V_{oc} mode) and IR thermography. Additional applied characterization tools were common characterization measurements [e.g., current-voltage (I-V) measurements].

3.1 Crystalline solar cells

3.1.1 Single cell module

The investigated single cell modules (without frame) includes a multi crystalline (mc) Si solar cell with glued connection wires (SnAg ribbon), an encapsulant (EVA), a front surface (standard glass) and a rear layer (three layer composite) (see Fig.2). The I-V measurement result of the two investigated single-cell-modules are shown in Figs.3 and Fig.4. The power output of the defect module was almost half compared to the power output of the single-cell-module without defects. The I-V curve also reveals that the defect module definitely has a very high series resistance.

As initial I-V measurements revealed that the power output of this single cell module was considerably low, optical measurements (EL, PL, and IR) were applied in addition to analyze the reason.

In the EL images (current applied ~I_{sc} and ~1/10 of I_{sc}) the defects (e.g., grain boundaries) or bus bars and fingers appear as dark areas.

In the EL-image of the single Si cell module a bright area appears in the upper right edge of the cell (next to the busbar) [see Fig. 5(a)]. The electron flow in this area is considerably

high. In order to identify, if this low electron flow in the remaining area of the cell is caused by material properties or by contacting problems, the performance of PL measurements was necessary. The PL-image shows that besides the grain boundaries no eye-catching material defects exist [see Fig. 5(b)]. Thus, it can be established that this inhomogeneous electron flow is not caused by material defects, but by contacting problems and higher series resistances. Finally, it turned out that only in the upper right edge of the cell (bright area) there is a good contact between the busbar and the flat ribbon.
The high electron flow is also viewable as hot area in the IR-image [see Fig. 5(c)]. However, if in this case only IR measurements were performed, the hot area in the IR-image could also be misinterpreted as defect (e.g., hot spot or short circuit).

2.1.2 Broken cell in a 60-cell-module

Figure 6(a) shows the EL image and Fig. 6(b) the PL image of a broken cell in a crystalline PV module (60-cell module, multi-crystalline cells, 245 W, from a two year old PV power plant in Italy).

The PL image gives more information about the material properties. Compared to the EL-image, electrically isolated areas can be better viewed and thus better analyzed. In parts of the isolated areas a bright contrast is produced, caused by the high electron flow and recombination in this area.

3.2 Thin film module (CIS)

A CIS-module (P_{max} 75 W, I_{sc} 2.4 A, Size: 605x1205x35 mm^2) was characterized by means of EL and IR measurements[15,26]. To determine the influence of defects (e.g., shunts) the EL behavior of the module when applying different current densities was investigated[27]. When applying a low current density the conductivity of shunts is very high. The stronger the shunts are the lower is the EL intensity in this area. Strong shunts are able to quench the EL intensity of a whole cell. When applying higher current densities, the conductivity of the pn-junction increases compared to the shunt conductivity, and shunts are less influential on the EL intensity distribution.

The EL images of the CIS module, taken after applying different forward bias voltages, were compared. Figure 7(b) shows the EL image of the CIS module with an injected current of 1A

(I_{sc} of the module) and Fig. 7(a) shows the EL image with an injected current of 0.1 A.
The comparison of the two EL images shows very clearly that effective shunts are visible as punctual defects and thus better detectable when high currents are injected. On the contrary the EL intensity of the area around effective shunts is considerably increased when low currents are injected.

Most identified defects (mainly shunts) in the EL image (Fig. 7) of the CIS-module are also visible in the dark thermography image [Fig. 8(a)]. The hot spots identified in Fig. 8(a) can be ascribed to areas with a low shunt resistance, where the current flows through the defect and creates a heat source.

Figure 8(b) shows the dark lock-in thermography image (amplitude image) of the CIS module. Compared to the dark IR-image [Fig. 8(a)], the DLIT-image of the CIS module is even more detailed. The identification of the defect position is further improved and the DLIT-image is even better comparable to the EL image (Fig. 7). The interpretation is the same.

In addition PL measurements were executed in order to further increase the defect analysis. An EL [Fig. 9(a)] and PL image [Fig. 9(b)] of the same section of the CIS module (marked with a black rectangle) were compared. It can be clearly seen that the defects are given in more detail in the PL-image. In the EL-image there are only dark areas with no exact position of the defect viewable. In the PL-image the exact position is determinable.

4. Conclusion

A very essential loss mechanism mainly for thin film modules is the loss due to localized shunts in the module. The existence of localized shunts respectively hot spots could be proofed in this work by means of EL and IR thermography measurements.

Finally, it could be proved that the effectiveness of defects (e.g., very strong shunts) is identifiable by means of current-dependent EL-measurements.
First performed PL measurements of CIS modules were compared with EL images and IR-images[28)]. A PL setup for the measurements of CdTe and a-Si modules is just built up at AIT.

PL images help to find out, if material defects or contacting problems are the reason for

power losses in solar cells and modules. Compared to EL images, PL imaging has the advantage that contacting failures do not influence the contrast of the PL images.
Furthermore, it could be demonstrated that PL imaging of solar cells and modules could be carried out successfully by means of LED excitation instead of hazardous and costly laser excitations. Thus, PL imaging could become a more interesting tool for the PV industry than EL imaging.

As the origin of a defect is not always located in the identified high temperature area or the remarkable dark EL areas, a combination of EL, PL, and IR techniques is necessary in order to identify as many defects as possible.

)

5. References

1) R. Ebner, “Non-destructive techniques for quality control of PV modules: infrared thermography, electro- and photoluminescence imaging”, 39th Annual Conference of the IEEE Industrial Electronics Society (2013).
2) S. Zamini, “Non-destructive-techniques for quality control of photovoltaic modules: electroluminescence imaging and infrared thermography”, Photovoltaics International, Journal, PVTECH Pro (2012).
3) R. Ebner, “Electroluminescence (EL) and infrared (IR) methods for characterizing different module technologies”, 26th European Photovoltaic Solar Energy Conference and Exhibition, Hamburg, Germany (2011).
4) R. Ebner, “EL an infrared IR methods for characterizing different thin-film module technologies”, Third International Conference, Thin Film PV, Munich, Germany (2011).
5) C. Buerhop, “Quality control of PV-modules in the field using infrared-thermography”, 26th EU-PVSEC, Hamburg, Germany (2011).
6) U. Hoyer, “Electroluminescence and infrared imaging for quality improvements of PV modules”, 23rd EU-PVSEC, Valencia, Spain (2008).
7) R. Ebner, “Electroluminescence (EL) and infrared (IR) methods for characterizing different thin-film module technologies”, Proc. 3rd Int. Conf. Thin Film PV, Munich, Germany, 2011.
8) A. Helbig, „Electroluminescence analysis of Cu(In,Ga)Se_2 thin-film modules“, 24th EU-PVSEC, Hamburg, Germany (2009).
9) U. Hoyer: “Electroluminescence and Infrared Imaging for Quality Improvements of PV Modules”, 23rd EU-PVSEC, Valencia, Spain (2008).
10) O. Breitenstein: “Lock-in thermography- basics and use for functional diagnostics of electronic components", Springer 2003, ISBN 3-540-43439-9.
11) O. Breitenstein, “Lock-in thermography- basics and use for functional diagnostic of electronic module technologies”, presented at the PV World Conf. & Expo, Tampa, Florida, USA (2011).
12) U. Hoyer, “Analysis of PV modules by electroluminescence and IR thermography”, 24th EU-PVSEC, Hamburg, Germany (2009).
13) M. Ankner, „Analyse von Fehlerbildern an Dünnschichtmodulen über das EL-Verfahren“, 25. PV-Symposium, Kloster Banz, Bad Staffelstein (2010)

)

14) M. Köntges, “Quantitative analysis of PV-modules by electroluminescence images for quality control”, 24th EU-PVSEC, Hamburg, Germany (2009).
15) T. Weber, “Electroluminescence investigation on thin film modules”, 26th EU-PVSEC, Hamburg, Germany (2011).
16) A. Mansouri, “Defect detection in photovoltaic modules using electroluminescence imaging”, Photovoltaic International (2010).
17) J.L. Crozier, “Identifying voltage dependant features in photovoltaic modules using electroluminescence imaging”, 29th EU-PVSEC, Amsterdam, Netherlands (2014).
18) G. Wang, “Failure analysis of dark cells detected by electroluminescence (EL)”, 28th EU-PVSEC, Amsterdam, Netherlands (2014).
19) R. Ebner: “Defect analysis in different photovoltaic modules using electroluminescence (EL) and infrared (IR)-thermography, 25th EU-PVSEC, Valencia, Spain (2010).
20) R. Ebner, “Electroluminescence (EL) and Infrared (IR) Imaging of Different Module Technologies”, PV-World Conference, Tampa, USA (2011).
21) A. Lawerenz, „Photoluminescence lifetime using LED arrays excitation source“, 25th PVSEC, Valencia, Spain (2010).
22) T. Trupke, “Fast photoluminescence imaging of Silicon wafers”, IEEE, 4th World Conference on PV Energy Conversion (2006).
23) A. Lawerenz, „Photoluminescence lifetime using LED arrays exitation source“, 25th PVSEC, Valencia, Spain (2010).
24) T. Trupke: “Fast photoluminescence imaging of Silicon wafers”, IEEE, 4th World Converence on PV Energy Conversion (2006).
25) M. Bailly, “Photoluminescence lifetime characterization with low pressure sodium lamps”, 28th EU-PVSEC, Paris, France (2013).
26) S. Johnston, “Imaging characterization techniques applied to Cu(In, Ga)Se2 solar cells”, J. Vac. Sci. Technol. A, Vol.28 (2010)
27) S. Roy, “Estimation of shunt resistance by electroluminescence imaging”, 29th EU-PVSEC, Amsterdam, Netherlands (2014).
28) R. Ebner: “Non-destructive techniques for quality control of PV-modules: infrared thermography, electro- and photoluminescence imaging”, IECON 2013, 39th Annual Conference of the IEEE Industrial Electronics Society (2013).

)

Figure captions:

Fig. 1. (Color online) PL setup at AIT.

Fig. 2. (Color online) Single-cell-module.

Fig. 3. (Color online) I-V curve of the defect single-cell module.

Fig. 4. (Color online) I-V curve of single-cell module without defects.

Fig. 5(a). (Color online) EL image.

Fig. 5(b). (Color online) PL image.

Fig. 5(c). (Color online) IR image.

Fig. 6(a). (Color online) EL image.

Fig. 6(b). (Color online) PL image.

Fig. 7(a). (Color online) CIS; EL (0.1 A).

Fig. 7(b). (Color online) CIS, EL (1 A).

Fig. 8(a). (Color online) CIS, IR.

Fig. 8(b). (Color online) CIS, DLIT.

Fig. 9(a). (Color online) CIS, EL.

Fig. 9(b). (Color online) CIS, PL.

)

Figures:

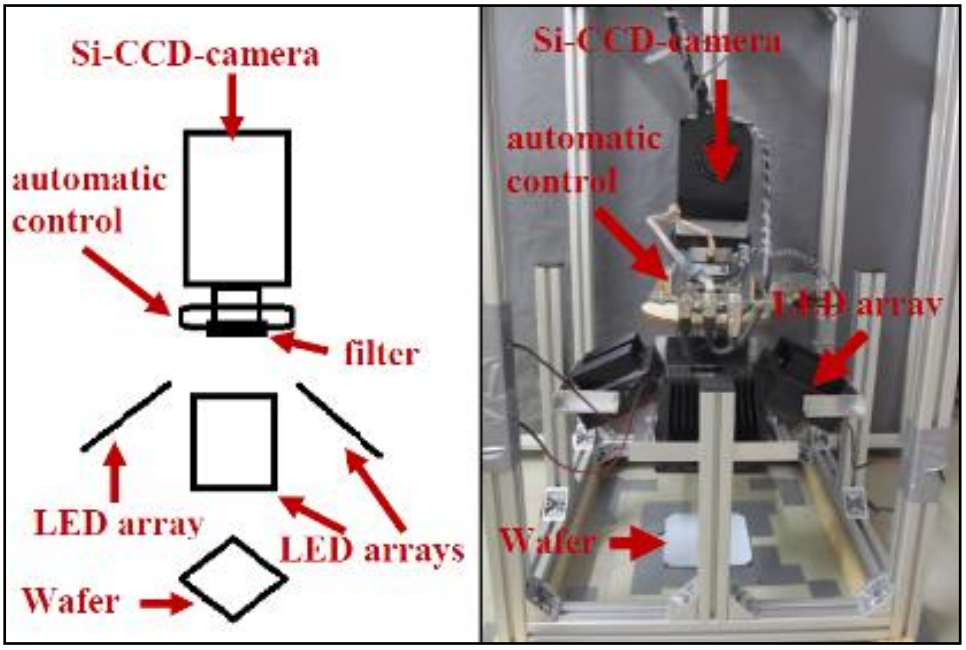

Fig. 1. PL setup at AIT.

Fig. 2. Single-cell-module.

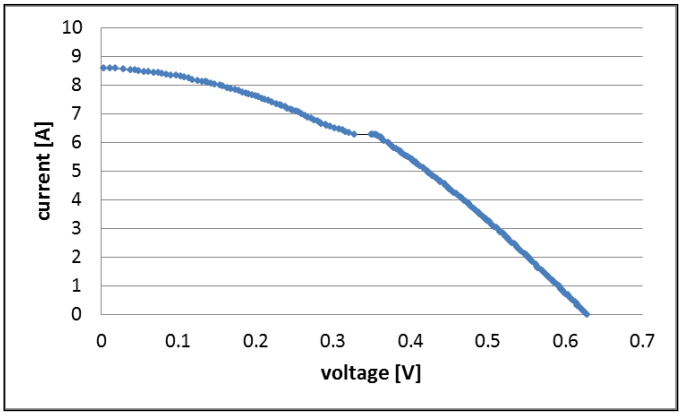

Fig. 3. I-V curve of the defect single-cell module.

)

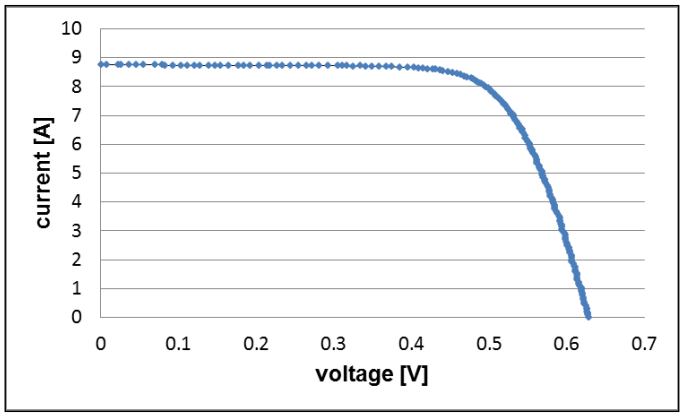

Fig. 4: I-V curve of single-cell module without defects.

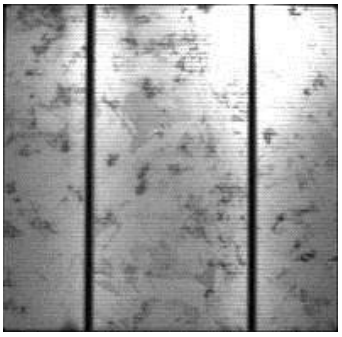

Fig. 5(a). EL image.

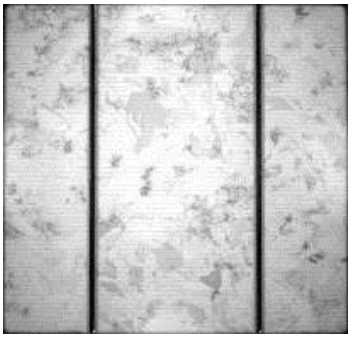

Fig. 5(b). PL image.

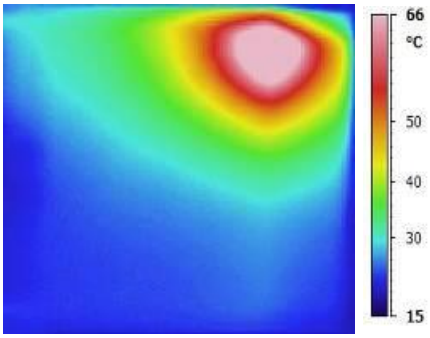

Fig. 5(c). IR image.

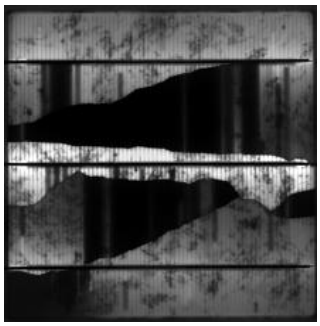

Fig. 6(a). EL image.

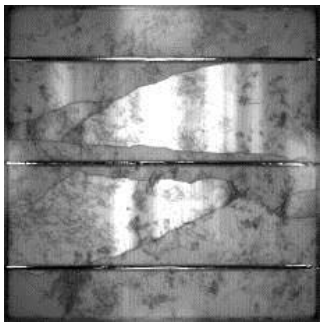

Fig. 6(b). PL image.

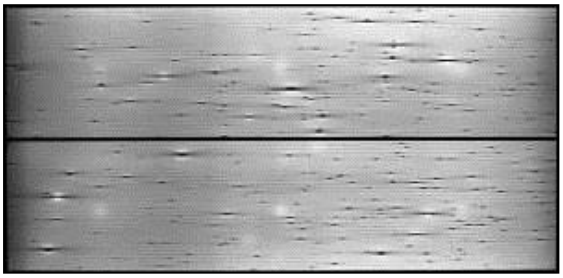

Fig. 7(a). CIS; EL (0.1 A).

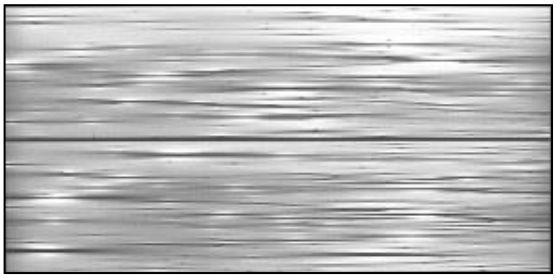

Fig. 7(b). CIS, EL (1 A).

)

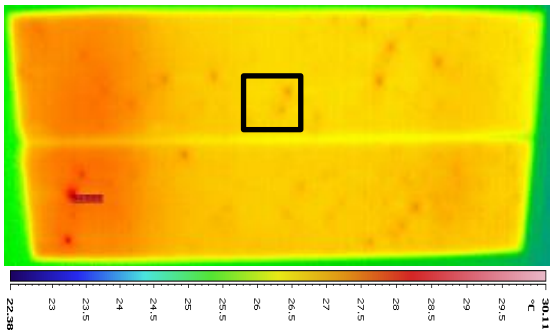

Fig. 8(a). CIS, IR.

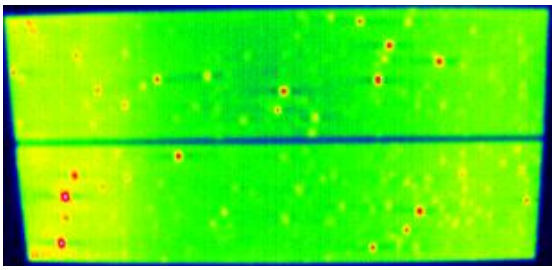

Temperature range: 0-0.35 Kelvin.

Fig. 8(b). CIS, DLIT.

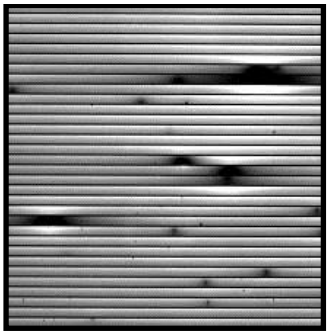

Fig. 9(a). CIS, EL.

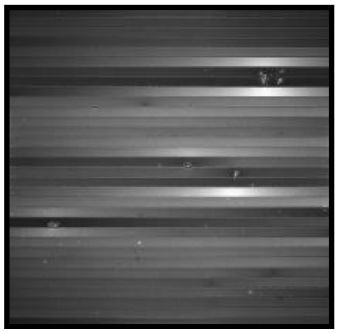

Fig. 9(b). CIS, PL.